

# Deep Reinforcement Learning for Sim-to-Real Policy Transfer of VTOL-UAVs Offshore Docking Operations

Ali M. Ali, Aryaman Gupta, and Hashim A. Hashim

arXiv:2406.00887v1 [cs.RO] 2 Jun 2024

**Abstract**—This paper proposes a novel Reinforcement Learning (RL) approach for sim-to-real policy transfer of Vertical Take-Off and Landing Unmanned Aerial Vehicle (VTOL-UAV). The proposed approach is designed for VTOL-UAV landing on offshore docking stations in maritime operations. VTOL-UAVs in maritime operations encounter limitations in their operational range, primarily stemming from constraints imposed by their battery capacity. The concept of autonomous landing on a charging platform presents an intriguing prospect for mitigating these limitations by facilitating battery charging and data transfer. However, current Deep Reinforcement Learning (DRL) methods exhibit drawbacks, including lengthy training times, and modest success rates. In this paper, we tackle these concerns comprehensively by decomposing the landing procedure into a sequence of more manageable but analogous tasks in terms of an approach phase and a landing phase. The proposed architecture utilizes a model-based control scheme for the approach phase, where the VTOL-UAV is approaching the offshore docking station. In the Landing phase, DRL agents were trained offline to learn the optimal policy to dock on the offshore station. The Joint North Sea Wave Project (JONSWAP) spectrum model has been employed to create a wave model for each episode, enhancing policy generalization for sim2real transfer. A set of DRL algorithms have been tested through numerical simulations including value-based agents and policy-based agents such as Deep Q Networks (DQN) and Proximal Policy Optimization (PPO) respectively. The numerical experiments show that the PPO agent can learn complicated and efficient policies to land in uncertain environments, which in turn enhances the likelihood of successful sim-to-real transfer.

**Index Terms**—Unmanned Aerial Vehicles, Offshore Docking, Reinforcement learning, Deep Q learning, Proximal Policy Optimization, Sim2Real.

## I. INTRODUCTION

### A. Motivation

VERTICAL Take-off and Landing Unmanned Aerial Vehicles (VTOL-UAVs) have been a standard part of offshore operations over the last few decades. VTOL-UAVs provide faster, safer, and more cost-efficient solutions for the inspection and maintenance of offshore operations for instance as in oil and gas facilities. The rapid growth of Micro-Electro-Mechanical Systems (MEMSs) contributed to the development of the VTOL-UAVs, however, there are still several challenges

to be solved [1], [2]. Flight endurance is a persisting challenge which limits the VTOL-UAV usage to only temporary missions in offshore operations [3]. Lithium polymer batteries are often used for UAV energy supply. Although Lithium batteries capacity has been improved over the last decade, they still provide a limited energy supply [4].

Offshore ocean operations can be accomplished through charging pads or docking stations with the capability to recharge or exchange lithium polymer batteries [5], [6]. Various designs of docking stations have been discussed in the literature, ranging from wireless charging pads to designs based on mechanisms of completely replacing the UAV battery [7]. Wireless charging stations free from human-based wired plugging/unplugging or replacing the batteries have been considered utilizing complicated mechanisms [8]. In [9]–[13] various wireless charging designs have been proposed with the merit of the lightweight and compact design of the charging pad. However, wireless charging stations are sensitive to misalignment leading to a reduction of power transmission efficiency. As an illustration, in the case of [14], the 200 Watt model exhibits a radial misalignment tolerance distance of merely 20 millimeters (mm). In [15] a wireless charging coupling structure was devised using copper tubes at both the transmitter and receiver. The transmission efficiency in [16] was 78%–80% within a radial misalignment of 32 cm to 44 cm. It becomes apparent that deploying a meticulous docking strategy can markedly decrease power loss during the charging phase.

The well-defined dynamic model of VTOL-UAVs motivated the active research community to formulate model-based controllers to decide either on static or moving platform docking operations [17], [18]. In [19], the VTOL-UAV was presumed to come with a basic sensor package comprising at least a camera and an inertial measurement unit, where the authors provided a rigorous analysis of system stability of the proposed controller based on Lyapunov functions. Vision-based nonlinear model predictive control (MPC) followed by boundary layer sliding mode was proposed in [20], where simulations and experiments showed successful landing in a moving platform with wind disturbances. Multi-sensor fusion techniques for localization have been utilized in the docking operations as in [21]–[23] for more precise docking. Despite the success of the model-based controllers, the architecture is handcrafted to solve specific situations and usually requires significant engineering effort and large computational power as in the case of MPC.

This work was supported in part by the National Sciences and Engineering Research Council of Canada (NSERC), under the grants RGPIN-2022-04937, RGPIN-2022-04940, DGEER-2022-00103 and DGEER-2022-00106.

A. M. Ali, A. Gupta, and H. A. Hashim are with the Department of Mechanical and Aerospace Engineering, Carleton University, Ottawa, ON, K1S-5B6, Canada (e-mail: hhashim@carleton.ca).

In recent years, the robotics community has extensively embraced Reinforcement Learning (RL) algorithms for controlling complex single-robot and multi-robot systems [24]–[28], establishing end-to-end policies, and in turn encompassing perception and control strategies [29]. RL’s foundation lies in emulating human trial-and-error learning, with agents acquiring knowledge through rewards obtained from their actions under various conditions. This reliance on rewards entails a significant number of episodes, thus exposing RL’s learning constraints concerning time and experience variability in real-world applications. The training of RL agents on real robots has been found to yield limited successes [30]–[32]. In contrast, contemporary RL algorithms have demonstrated remarkable performance when trained with ample amounts of inexpensive synthetic data from virtual experiments. Consequently, a prevalent strategy in learning schemes involves conducting agent training within simulated environments that closely approximate real-world conditions [33]–[39].

In [40], [41] Deep Reinforcement Learning (DRL) has been employed in conventional control problems related to VTOL-UAV, encompassing attitude control, set-point tracking, hovering, and disturbance recovery. Utilizing a low-resolution camera facing downward, a Deep-Q Network (DQN) identified a marker and successfully executed a landing in [42]. A Deep Deterministic Policy Gradient (DDPG) algorithm was implemented to guide a VTOL-UAV for landing on a moving platform [42]–[44]. In [45], the study addresses the challenging task of landing a VTOL-UAV on inclined surfaces, where conventional control methods are not applicable due to the non-equilibrium nature of the final state. Unfortunately, current DRL docking schemes exhibit drawbacks, including lengthy training times, and modest success rates. The lengthy training times arise from learning complicated three-dimensional (3D) navigation policies, while the primary cause of modest success rates lies in the disparity between the simulated environment and real-world conditions.

*Contributions:* Inspired by the limitations found in the literature on DRL-based docking of VTOL-UAV schemes, the paper contributions can be outlined as follows:

- Unlike [40], [41], the docking task of VTOL-UAV is decomposed into a sequence of more manageable but analogous phases. The approach phase and the landing phase reduce the training time. Also, the proposed learning architecture learns the optimal policy to land on a docking platform considering uncertainty and unknown movement in the docking landing phase; in contrast to [40], [41] which focus on stable and static docking platform.
- A novel generalized policy for sim-to-real transfer based on domain randomization has been provided to increase the success rates in landing operations. The DRL agents learn using a virtual environment subjected to a randomized disturbance describing the hydrodynamic waves represented by the Joint North Sea Wave Project (JONSWAP) spectrum model.
- A set of policy-based and value-based DRL agents have been tested with respect to learning stability against the randomized disturbance.

*Organization:* The remaining part of the paper is organized as follows: Section II presents preliminaries on DRL. The Problem formulation is stated in Section III along with the proposed DRL agents and the randomized disturbance virtual environment. Section IV illustrates the performance of the proposed learning agents scheme through numerical simulations. Finally, Section V concludes the work.

## II. PRELIMINARIES

### A. Deep Reinforcement Learning

Let  $\mathbb{R}$  be the set of real numbers and  $\mathbb{Z}^+$  be the set of non-negative integers. A finite Markov decision process is a stochastic control process in discrete time, represented as a 4-tuple such that  $\text{MDP} = (S, A, p, r)$  where:

- $S$  is set of a finite number of states.
- $A$  is set of a finite number of actions.
- $r : S \times A \rightarrow \mathbb{R} : r(s'|s, a)$  is the expected instantaneous reward obtained upon transitioning from state  $s \in S$  to a new state  $s' \in S$ , due to action  $a \in A$  where  $|$  denotes the notation of the conditional probability.

The reward can be written as:

$$r(s, a) = \sum_{r \in \mathbb{R}} r \sum_{s' \in S} p(s', r|s, a)$$

- $p : S \times A \times S \rightarrow [0, 1]$  is the state transition probability where action  $a$  in state  $s \in S$  at time  $t \in \mathbb{Z}^+$  leads to state  $s' \in S$  at time  $t + 1$ .  $p$  can be defined as:

$$p(s', r|s, a) = \sum_{r \in \mathbb{R}} p(s', r|s, a)$$

In reinforcement learning, the fundamental aim is formalized through a reward signal transferred from the environment to the agent at each time step  $r_t \in \mathbb{R}$ . The agent’s goal is to maximize the total cumulative reward received over the long run, which means not maximizing the immediate reward. The agent endeavors to devise a policy for decision-making that maximizes the cumulative discounted reward anticipated in the future. The expected discounted return  $R$  at time  $t \in \mathbb{Z}^+$  is defined as follows:

$$R_t = \mathbb{E} \left[ \sum_{k=0}^{\infty} \gamma^k r_{t+k+1} \right] \quad (1)$$

where  $0 \leq \gamma \leq 1$  is the discount factor and  $k$  is the time step. Let  $V_{\pi}(s)$  be the value of a state  $s$  under a policy  $\pi$ ; and it represents the expected return when starting in the state  $s$  such that:

$$V_{\pi}(s) = \mathbb{E}_{\pi} \left[ \sum_{k=0}^{\infty} \gamma^k r_{t+k+1} | s_t = s \right] \quad (2)$$

where  $\mathbb{E}_{\pi}[\cdot]$  represents the expected value of a random variable given that the agent adheres policy  $\pi$ . In this manner, the value of taking action  $a$  in state  $s$  under a policy  $\pi$ , denoted by  $Q_{\pi}(s, a)$  and it is termed the action value function. It defines the expected return starting from  $s$  taking action  $a$  and following a policy  $\pi$  such that:

$$Q_{\pi}(s, a) = \mathbb{E}_{\pi} \left[ \sum_{k=0}^{\infty} \gamma^k r_{t+k+1} | s_t = s, a_t = a \right] \quad (3)$$

from Eq. (2) and (3) the advantage function  $A_\pi(s, a)$  can be defined as follows:

$$A_\pi(s, a) = Q_\pi(s, a) - V_\pi(s) \quad (4)$$

Given an estimate of  $Q_\pi(s_t, a_t)$ , it is possible to enhance the policy by, for instance, acting greedily based on  $Q_\pi(s_t, a_t)$  for instance:

$$\pi'(s_t) = \operatorname{argmax}_a Q_\pi(s_t, a). \quad (5)$$

where  $\pi'(s_t)$  is the improved policy. The conventional Q Learning algorithm conducts policy evaluation through temporal difference estimation and adjusts the  $Q$  estimation according to the Bellman Eq. [46] as follows:

$$Q_\pi^{\text{new}}(s_t, a_t) = Q_\pi^{\text{old}}(s_t, a_t) + \alpha(r_t + \gamma \max_a Q_\pi^{\text{old}}(s_{t+1}, a) - Q_\pi^{\text{old}}(s_t, a_t)) \quad (6)$$

where  $\alpha \in \mathbb{R}$  refers to a step size. The conventional standard tabular Q-learning method is challenged by the curse of dimensionality, rendering computationally intractable in scenarios where the number of states and actions grows substantially, a common occurrence across various practical applications. An alternative approach leveraging artificial neural networks for estimating the  $Q$  function, giving rise to the DQN algorithm as initially proposed in [47]. Algorithms that aim to estimate the  $Q$  function and subsequently make decisions based on the current estimation fall into the category of value-based algorithms, while if we directly learn the optimal policy  $\pi_\theta^*$  through a neural network that maximizes a given objective function that will be called policy based algorithms.

### III. PROBLEM FORMULATION

This Section aims to formulate DRL agents to learn the optimal policy that enables a safe and accurate landing on an offshore docking station subjected to disturbance. Define  $\{\mathcal{I}\}$  as the inertial frame coordinates and  $\{\mathcal{B}\}$  as the body frame coordinates. Recall the mapping between a rotational matrix  $R \in SO(3)$  to Euler angles  $\zeta = [\phi, \theta, \psi]^\top \in \mathbb{R}^3$  ( $R \rightarrow \zeta$ ) and vice versa  $\zeta \rightarrow R$  where  $SO(3)$  refers to the Special Orthogonal Group of order 3 (for more information visit [1]):

$$R_\zeta = \begin{bmatrix} c_\psi c_\theta & c_\psi s_\phi s_\theta - c_\phi s_\psi & s_\phi s_\psi + c_\phi c_\psi s_\theta \\ c_\theta s_\psi & c_\phi c_\psi + s_\phi s_\psi s_\theta & c_\phi s_\psi s_\theta - c_\psi s_\phi \\ -s_\theta & c_\theta s_\phi & c_\phi c_\theta \end{bmatrix}. \quad (7)$$

The dynamics of a rigid body subject to external forces applied to its center of mass and articulated in Newton-Euler formalism is delineated as follows:

$$\sum F = m\dot{V}, \quad F, V \in \{\mathcal{I}\} \quad (8)$$

$$\sum M = J\dot{\Omega} + \Omega \times J\Omega \quad M, \Omega \in \{\mathcal{B}\} \quad (9)$$

where  $V = [v_x \ v_y \ v_z]^\top \in \mathbb{R}^3$  is the UAV linear velocity vector in the inertial frame  $\{\mathcal{I}\}$ ,  $\Omega = [\Omega_x \ \Omega_y \ \Omega_z]^\top \in \mathbb{R}^3$  describes UAV rotational velocity in the body frame  $\{\mathcal{B}\}$ ,  $m$  is the total mass of the UAV,  $J$  refers to the inertia matrix, and  $\times$  denotes the cross product between two vectors.  $\sum F$

and  $\sum M$  are the sum of the external forces and moments acting on the VTOL-UAV. To facilitate the formulation of a learning framework, our aim is to decompose the docking into two phases; the approach phase and the landing phase as illustrated in Figure 1. The approach phase is a 3D navigation and tracking control problem, which can be successfully addressed by the rich literature on such problems (e.g., [48], [49]). In [48] and [49], the authors used known landmarks obtained through a vision-aided unit (monocular or stereo camera) and an Inertial Measurement Unit (IMU). This enabled the development of an observer-based controller with exponential stability, facilitating effective 3D navigation and tracking control for VTOL-UAVs. Utilizing model-based control schemes in the approach phase is reasonable since the model of VTOL-UAV is known, and there are no significant advantages in learning a complicated policy using model-free DRL agents. Nevertheless, the adaptation of the model-based control in the approach phase will provide a more manageable learning task in the landing phase. The landing phase will start when the approach phase is finished, where the VTOL-UAV will navigate in 3D space and align with the docking station with a fixed height denoted by  $H_0$ . The DRL agents learn the optimal policy to drive the VTOL-UAV to land accurately with minimal impact force against the disturbed docking station. Learning offline in a simulated environment with a randomized disturbance will provide an optimal generalized policy in terms of neural network mapping the current state to the optimal action providing fast online solutions.

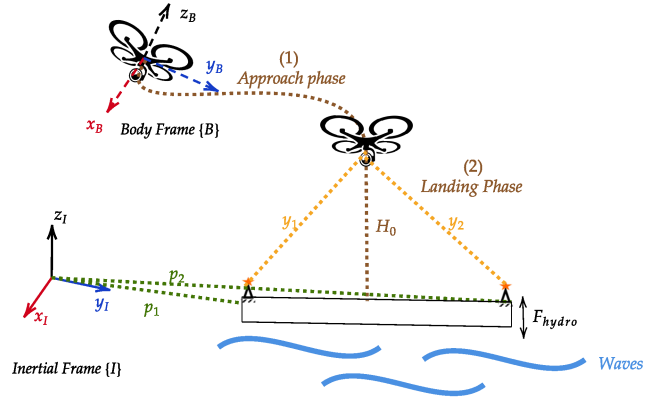


Fig. 1: VTOL-UAV landing task on an offshore landing pad, where  $\{\mathcal{B}\}$  refers to the body-fixed frame and  $\{\mathcal{I}\}$  is the Inertial-frame. The distances  $\{y_1, y_2\}$  are from the VTOL-UAV to the landmarks attached to the docking station to be used in the approach phase. The distances  $\{p_1, p_2\}$  are from the inertial frame to the corners of the landing pad. For more information about the approach phase using landmark please refer to [49], [48].

#### A. Environment

This subsection aims to develop a mathematical framework for a virtual environment representing the landing phase, tasked with training the DRL agents offline. In the view of

Eq. (8), the sum of the external forces  $\sum F$  can be written as follows:

$$\sum F = \underbrace{\begin{bmatrix} 0 \\ 0 \\ -mg \end{bmatrix}}_{\text{gravity}} + R_{\zeta} \underbrace{\begin{bmatrix} 0 \\ 0 \\ U_1 \end{bmatrix}}_{\text{total-thrust}} \quad (10)$$

As such, from Eq. (10) the vertical dynamics of the VTOL UAV can be described by:

$$z \rightarrow \dot{x}_1 = x_2 \quad (11)$$

$$\dot{z} \rightarrow \dot{x}_2 = \frac{-k_{fdz}}{m}x_1 - g + U \quad (12)$$

where  $x = [x_1 \ x_2]^\top$ ,  $x_1 = z$ ,  $x_2 = \dot{z}$ ,  $k_{fdz}$  denotes the aerodynamic drag coefficient in the  $z$  direction, and  $U$  refers to the virtual control direction acting on the direction of  $z_b$  such that the actual thrust  $u = \frac{m}{c_\phi c_\theta}U$ . Starting from initial height  $H_0$  and assuming that VTOL-UAV is perfectly aligned from the approach phase lead to  $c_\phi = c_\theta = 1$ , one finds the stabilizing hover controller as follows:

$$U_0 = \frac{k_{fdz}}{m}x_1 + g.$$

The formulation of the DQN agents requires a discrete action space, unlike the Proximal Policy Optimization (PPO) agent which can accommodate continuous action space. The discrete action space is defined by  $A_d = [U_+, U_0, U_-]$  where  $U_+$  and  $U_-$  refers to the set of control values with a bigger and smaller values with respect to  $U_0$ , respectively. The continuous action is defined by  $A_c = \{U : U_{\min} \leq U \leq U_{\max}\}$  where  $U_{\min}$  and  $U_{\max}$  are the minimum and maximum values of the virtual control input, respectively. The state space  $S = [z - z_w \ \dot{z}]^\top \in \mathbb{R}^2$  is defined for both DQN and PPO agents, where  $z_w$  is the vertical displacement of the docking platform due to the  $F_{\text{hydro}}$  to be defined subsequently. The dynamics in Eq. (11) and (12) will be numerically integrated using the SciPy [50] Adams/backward differentiation formula methods in Python at each time step. The docking station position at the origin is subjected to a stochastic noise from the hydrodynamic waves  $F_{\text{hydro}}$ . The JONSWAP spectrum is a widely utilized model in oceanography and engineering for describing the energy distribution in ocean waves [51]. It is characterized by a peak enhancement at a certain frequency and a rapid decrease in energy at frequencies away from the peak. The JONSWAP spectrum is described by:

$$S(f) = \frac{\alpha_w g^2}{k_w^4} (f)^{-5} e^{(-\frac{5}{4}(\frac{f}{f_p})^4)} \gamma_w e^{\frac{(-\frac{f-f_p}{2\sigma^2 f_p^2})^2}{2\sigma^2 f_p^2}} \quad (13)$$

where  $f$  is the wave frequency,  $S(f)$  represents the spectral energy density at a wave frequency  $f$ ,  $\alpha_w$  is the Phillips constant, which is typically set as 0.0081 for deep water,  $k_w$  is the von Karman constant set as 0.016 for deep water,  $f_p$  is the peak frequency at which the spectrum has the maximum energy,  $\gamma_w$  is a dimensionless shape parameter that helps to define the shape of the spectrum, and  $\sigma$  is the spectral width parameter, which influences the width of the spectrum. The Fourier transform  $X(\omega)$  of the spectrum is obtained, followed

by the generation of the time domain wave using the inverse Fourier transform such that:

$$X(f) = \int_{-\infty}^{\infty} S(f) e^{-2\pi f t} df \quad (14)$$

where the magnitude is given by  $|X(\omega)| = \sqrt{\text{Re}(X(\omega))^2 + \text{Im}(X(\omega))^2}$  and the phase is defined by  $\phi_\omega = \tan^{-1}(\frac{\text{Im}(X(\omega))}{\text{Re}(X(\omega))})$ . A random value  $\phi_\omega = [0, 2\pi]$  is used to generate a random wave single for each episode. This results in a random time domain signal that represents the desired wave such that  $z_w(t) = \mathcal{F}^{-1}[X(\omega)]$ , where  $\mathcal{F}^{-1}$  is the inverse Fourier transform and  $z_w$  is the landing position disturbed by the hydrodynamic waves.

## B. Reward

The formal definition of a reinforcement learning problem necessitates the specification of the reward function. In this work, the reward function is formulated to give a higher reward to the VTOL-UAV while approaching the landing pad and minimizing the impact force. Define  $e_p = z - z_w$  and  $e_v = \dot{z} - \dot{z}_d$  to be the error in height and height rate, respectively. In order to maintain a soft landing with minimal impact force, one can assign the required velocity  $\dot{z}_d$  to do so (e.g., exponential decay of the required velocity). The proposed reward function can be defined as follows:

$$R(s, a) = -k_1 e_p - k_2 e_v. \quad (15)$$

where  $k_1$  and  $k_2$  are gain constants to give more weight of  $e_p$  or  $e_v$  within the reward value.

## C. Value based Agents

The fundamental concept underlying value-based reinforcement learning algorithms is to iteratively update and estimate the action-value function  $Q$  in Eq. (3) using the Bellman equation as follows:

$$Q_{k+1}(s, a) = \mathbb{E}[R + \gamma \max_{a'}(s', a') | s, a] \quad (16)$$

Conventional tabular value-based algorithms converge to the optimal action value function,  $Q_k \rightarrow Q^*$  as  $i \rightarrow \infty$  [52]. In practice, tabular value-based algorithms is computationally untraceable, due to the issue of dimensionality arising from the vast number of possible values of states  $(z, \dot{z})$ . Alternatively, it is typical to employ a function approximator to estimate the action-value function, denoted as,  $Q(s, a; \theta) \approx Q^*(s, a)$ .

1) *DQN*: A neural network function approximator with parameters represented by  $\theta$  is referred to as a  $Q$  network. In [47], a  $Q$  network can be trained by minimizing a sequence of loss functions  $\mathcal{L}_k(\theta_k)$  defined in Eq. (17) that changes at each iteration  $k$ .

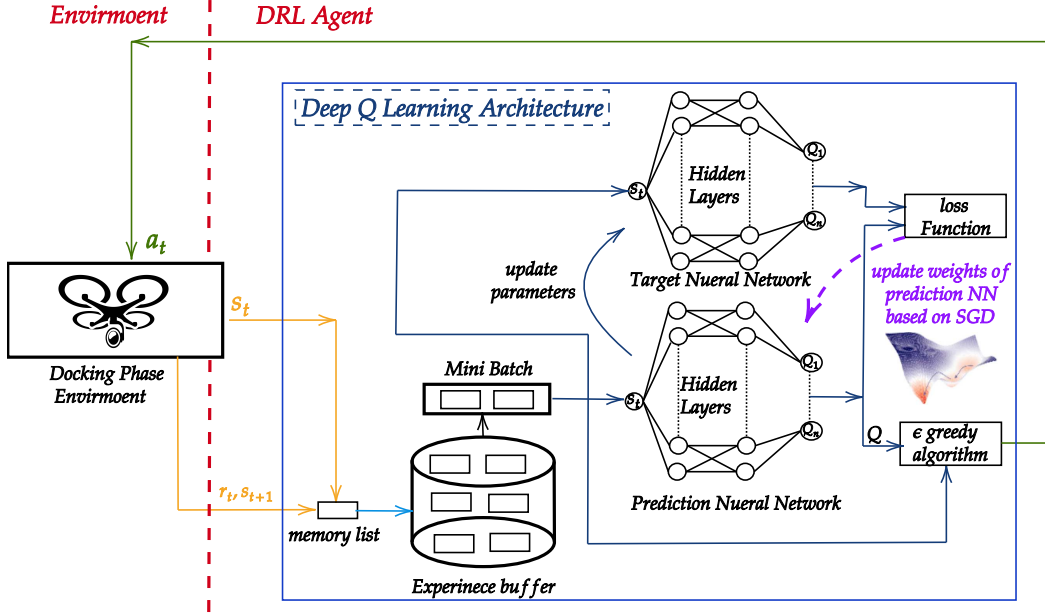


Fig. 2: DQN Agent architecture interacting with the docking phase environment.

---

### Algorithm 1 DQN Docking Learning Algorithm

---

**Input:**  $M, C, F, \gamma, \epsilon_0, \epsilon_f, \alpha, f_p,$  and  $\gamma_w$ .

**Output:**  $\theta$

**Initialization:**

1: Initialize  $\theta_{\text{prediction}}$ , and  $\theta_{\text{target}}$ .

**for** every episode =  $1, \dots, M$  **do**

5: Initialize  $s_1$  and  $\theta_{\text{prediction}} = \theta_{\text{prediction}}(s_1)$ .

6: Compute  $|X(\omega)| = \sqrt{\text{Re}(X(\omega))^2 + \text{X}(f(\omega))}$  from Eq. (13) and (14).

7: Generate a random phase  $\phi_\omega = [0, 2\pi]$ .

8: Generate the wave time signal from  $z_w(t) = \mathcal{F}^{-1}[X(\omega)]$ .

**for** every time step  $k = 1, \dots, k_f$ .

9: Every  $F$  Steps set  $\theta_{\text{prediction}} = \theta_{\text{target}}$ .

10: compute a random number  $\zeta \sim \text{Uniform}(0, 1)$ .

**if**  $\zeta > \epsilon$  **then**

11: select  $a_k = \text{argmax}_{a' \in A(s_t)} Q(s_k, a', \theta_{\text{prediction}})$ .

**else**

12: select a random action  $a_k \in A$ .

**end if**

13: Apply the action  $a_k$ .

14: Numerically integrate the dynamics in Eq. (11) and (12) using SciPy.

15: Store  $(s_k, a_k, r_k, s_{k+1})$  in  $D$ .

16: Sample a random mini batch of  $(s_j, a_j, r_j, s_{k+1})$  from  $D$ .

17: Set  $Q_j = r_j + \gamma \max_{a'} Q(\phi_{j+1}, a'; \theta_{\text{target}})$

18: execute a gradient descent step to minimize

$$\mathcal{L} = (Q_j - Q(s_j, a_j; \theta_{\text{prediction}}))^2$$

19: update  $\theta \leftarrow \theta + \alpha \nabla_{\theta} J(\theta)$ .

**end for**

**end for**

20: Save  $\theta_{\text{prediction}}$

---

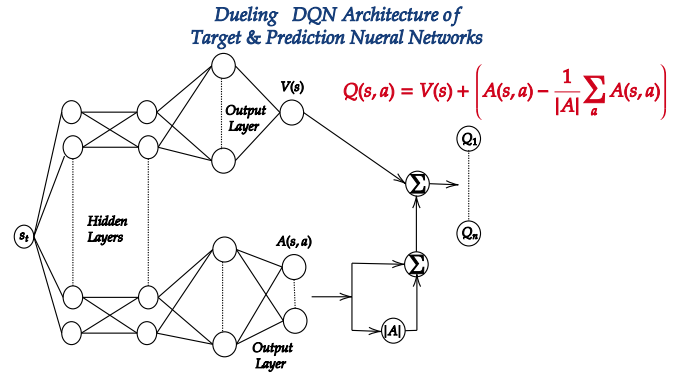


Fig. 3: Dueling Architecture of Target & Prediction Neural Networks.

$$\mathcal{L}_k(\theta_k) = (y_k - Q(s_k, a_k; \theta_{\text{prediction}}))^2 \quad (17)$$

where  $y_k = r + \gamma \max_{a'} Q(s', a'; \theta_{k-1})$  is the target for time step  $k$ . The weights from the previous time step  $\theta_k$  are held fixed when optimizing the loss function  $\mathcal{L}_k(\theta_k)$ . It is worth noting that the targets are contingent on the network weights. This differs from the fixed targets employed in supervised learning, which remain unchanged before the learning process commences. Stochastic Gradient Descent (SGD) can be utilized to minimize the loss function in (17). Using the experience replay technique, the agent's experiences at each time step will be a sequence of  $(s_k, a_k, r_k, s_{k+1})$  stored in memory  $D$  with capacity  $C$ . The JONSWAP spectrum wave model is embedded in the calculation of the dynamics of the environment. Within the inner loop of the algorithm,  $Q$  values updates and mini-batch updates are applied to randomly sampled experiences from the stored pool. Following the completion of experience replay, the agent chooses and executes an action based on an  $\epsilon$ -greedy policy. The details of

the implementation of the algorithm are shown in Algorithm 1 and Figure 2.

*Algorithm 1 Discussion:* The algorithm begins by initializing essential components such as the replay memory with capacity  $C$ , number of episodes  $M$ , update frequency  $F$ , discount factor  $\gamma$ , initial exploration  $\epsilon_0$ , final value  $\epsilon_f$ , learning rate  $\alpha$  and other parameters identifying the wave spectral energy in Eq. (13) as  $\alpha_w, f_p$ , and  $\gamma_w$ . It then proceeds to iterate through each episode, computing the magnitude of the Fourier Transform in Eq. (14) and generating a random phase before deriving the time-domain wave signal from the inverse Fourier transform. Within each time step, the algorithm updates the prediction neural network every  $F$  steps to match the target network, selects an action based on the current state and neural network predictions, and applies this action to the system. It then stores the resulting transition in the replay memory and samples a random mini-batch of transitions for further processing. Utilizing the Bellman equation, the algorithm updates the  $Q$ -value, performing a gradient descent step to minimize the loss in Eq. (17). The neural network weights are then updated accordingly, and the final learned weights that represent the policy learned are saved for future use for Sim-to-Real implementation.

2) *Double DQN:* The previously mentioned  $Q$ -learning algorithm is known to overestimate action values. In both  $Q$ -learning and DQN, the max operator in (16) utilizes identical values for both selecting and evaluating an action. This raises the probability of selecting values that are overestimated, resulting in overly optimistic estimations of value. To address this issue, we can separate the selection process from the evaluation. In the case of Double DQN [53], two value functions are trained by randomly assigning experiences to update either of the two value functions, yielding two sets of weights,  $\theta$  and  $\theta'$ . During each update, one set of weights is employed to establish the greedy policy, while the other is utilized to assess its value. This decoupling of selection and evaluation allows for a clear comparison, aligning with the principles of  $Q$ -learning.

3) *Dueling DQN:* Starting with the standard DQN architecture, it is possible to divide the network into two distinct streams: one dedicated to estimating the state value, and the other focused on assessing state-dependent action advantages. Following the two streams, the final module of the network merges the outputs of state value and advantage, illustrated in Figure 3. The approach introduced in [54] suggests that the last module of the neural network executes the forward mapping as follows:

$$Q(s, a; \theta, \alpha, \beta) = V(s; \theta, \beta) + (A(s, a; \theta, \alpha) - \frac{1}{|A|} \sum_{a'} A(s, a'; \theta, \alpha)) \quad (18)$$

The dueling architecture maintains an identical input-output interface as the standard DQN architecture, ensuring an identical training process. The Dueling DQN loss function can be expressed in terms of mean squared error, such as:

$$\mathcal{L} = \frac{1}{N} \sum_{i \in N} (Q_j - Q(s_j, a_j; \theta_{\text{prediction}}))^2 \quad (19)$$

## D. Policy based Agents

---

### Algorithm 2 PPO Docking learning Algorithm.

---

**Input:**  $M, C, \gamma, \alpha_{\text{critic}}, \alpha_{\text{actor}}, \alpha_w, f_p$ , and  $\gamma_w$ .

**Output:**  $\theta$

**Initialization:**

1: Initialize  $\theta_{\text{actor}}$  and  $\theta_{\text{critic}}$ .

**for** every episode =  $1, \dots, M$  **do**

4: Initialize  $s_1$ .

5: Compute  $|X(\omega)| = \sqrt{\text{Re}(X(\omega))^2 + X(f(\omega))}$  from Eq. (13) and (14).

6: Generate a random phase  $\phi_\omega = [0, 2\pi]$ .

7: Generate the wave time signal from  $z_w(t) = \mathcal{F}^{-1}[X(\omega)]$ .

**for** every time step  $k = 1, \dots, k_f$

8: Select  $a_k$  according to old policy  $\pi(s_k | \theta_{\text{old}})$ .

9: Numerically integrate the dynamics in Eq. (11) and (12) using SciPy.

10: Store  $(s_k, a_k, r_k, s_{k+1})$  in  $D$ .

11: Calculate the estimates  $A_1, \dots, A_{k_f}$  according to (put the equation here).

**end for**

**for** each epoch

12: Sample a random mini batch of  $L$  transitions from  $D$ .

13: execute a gradient descent step to minimize  $\mathcal{L}^V = \hat{E}[(\hat{V}_{\theta_{\text{critic}}}(s_k) - V_{\theta_{\text{critic}}}(s_k))^2]$ .

14: execute a gradient descent step to minimize  $\mathcal{L}^{\text{PPO}} = \hat{E}[\min(R_k(\theta_{\text{actor}}), \text{clip}(R_k(\theta_{\text{actor}}), 1 - \epsilon_{\text{PPO}}, 1 + \epsilon_{\text{PPO}})) \hat{A}_k]$ .

15: update  $\theta_{\text{critic}} \leftarrow \theta_{\text{critic}} + \alpha_{\text{critic}} \nabla_{\theta} J(\theta_{\text{critic}})$ .

16: update  $\theta_{\text{actor}} \leftarrow \theta_{\text{actor}} + \alpha_{\text{actor}} \nabla_{\theta} J(\theta_{\text{actor}})$ .

**end for**

**end for**

17: save  $\theta_{\text{actor}}$

---

1) *Proximal Policy Optimization (PPO):* The PPO algorithm, introduced in [55], is a policy gradient method applicable to environments featuring both discrete and continuous action spaces. It trains a stochastic policy using the on-policy actor-critic method. The actor maps observations into actions, while the critic provides an expected reward for the given observation. Initially, it gathers a set of trajectories per epoch by sampling from the most recent version of the stochastic policy. The policy undergoes updates through SGD optimization, whereas the value function is adjusted using a gradient descent algorithm.

Define  $\delta_k = r_k + \gamma V(s_{k+1}) - V(s_k)$ . The Generalized Advantage Estimator (GAE) can be computed as follows [56]:

$$\hat{A}_k = \delta_k + (\gamma\lambda)\delta_{k+1} + (\gamma\lambda)^2\delta_{k+2} + \dots + (\gamma\lambda)^{\mu-k+1}\delta_{\mu-1} \quad (20)$$

where  $\mu$  is the sampled mini-batch size and the loss function of the policy gradient can be expressed as

$$\mathcal{L} = \hat{E}[|\hat{V}_k^{\text{target}}(s_k) - V_k(s_k)|] \quad (21)$$

where  $\hat{V}_k^{\text{target}}(s_k) = r_{k+1} + \gamma V_k(s_{k+1})$  and the weights of the policy neural network will be updated by an SGD algorithm.

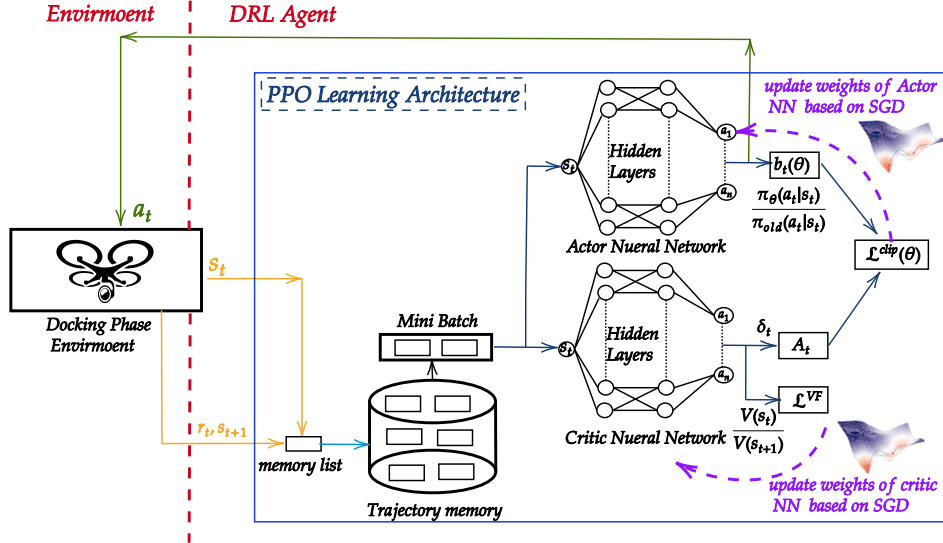


Fig. 4: PPO Agent architecture interacting with the docking phase environment.

In [57] Trust Region Policy (TRP) utilized the loss function with respect to the following constraint:

$$\hat{E}[KL[\pi_{old}(\cdot|s_k), \pi_{\theta}(\cdot|s_k)]] \leq \delta_0 \quad (22)$$

where  $\delta_0$  is a small number and  $KL$  is the kullback-leibler divergence defined in [57]. The PPO algorithm in [55] has the same idea as the TRP but it is much simpler to be implemented with better sample efficiency. Define the probability ratio  $R_k(\theta) = \frac{\pi_{\theta}(a_k|s_k)}{\pi_{old}(a_k|s_k)}$ . The PPO loss function is given by

$$\mathcal{L}^{PPO}(\theta_{actor}) = \hat{E}[\min(R_k(\theta_{actor}), \text{clip}(R_k(\theta_{actor}), 1 - \epsilon_{PPO}, 1 + \epsilon_{PPO}))\hat{A}_k)] \quad (23)$$

where  $\epsilon$  is the clipping parameter. The clipped objective function  $\mathcal{L}^{PPO}$  prevents PPO from exhibiting a bias towards actions with positive advantages and enables it to promptly steer clear of actions associated with a negative advantage function within a mini-batch of samples. The parameters of  $\pi_{\theta}$  are updated by an SGD algorithm with the gradient  $\Delta \mathcal{L}^{PPO}$ . The update of the critic and actor weights is done using SGD as follows:

$$\theta_{actor} = \theta_{actor} - \alpha_{actor} \nabla \mathcal{L}^{PPO}(\theta_{actor}) \quad (24)$$

$$\theta_{critic} = \theta_{critic} - \alpha_{critic} \nabla \mathcal{L}^{PPO}(\theta_{critic}) \quad (25)$$

where  $\alpha_{actor}$  and  $\alpha_{critic}$  are the learning rate of the actor and critic respectively.

*Algorithm 2 Discussion:* The algorithm begins by initializing the replay memory with capacity  $C$ , number of episodes  $M$ , discount factor  $\gamma$ , learning rate of the actor and critic neural networks  $\alpha_{critic}$ ,  $\alpha_{actor}$ , and other parameters identifying the wave spectral energy in Eq. (13) as  $\alpha_w$ ,  $f_p$ , and  $\gamma_w$ . In steps 4-7, the random wave in the time domain is generated within each epoch as shown in Eq. (13) and (14). For each time step, it samples a random mini-batch of transitions from the memory and updates the Critic network by minimizing

the value function loss and the actor-network using the PPO loss described in Eq. (23). Both networks (actor and critic model) are updated using SGD with the learning rates  $\alpha_{critic}$  and  $\alpha_{actor}$ . The final weights of the actor-network are saved as  $\theta_{actor}$  representing the policy learned.

#### IV. NUMERICAL RESULTS

In this section, the main results will be discussed. The computing source used to carry out simulations in this section has the following specifications: Windows 11 (64-bit processor), CPU (Intel(R) i7-10760H, 2.60GHz, 2592 MHz, 6 core, and 12 logic processors), and 16 GB RAM. The  $\epsilon$  greedy value

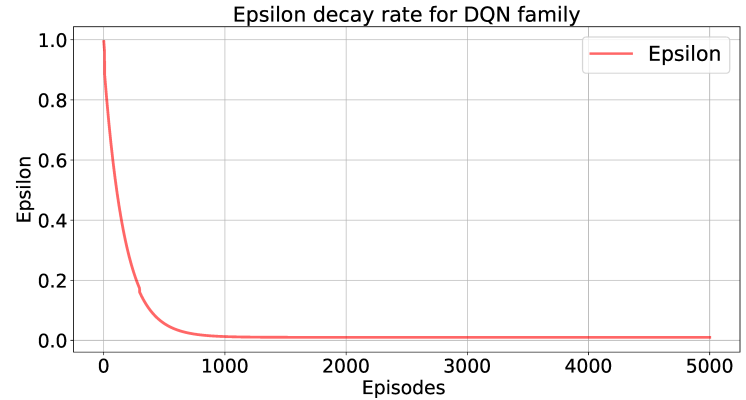


Fig. 5: The  $\epsilon$  greedy value used in DQN agents. The initial and final greedy values were  $\epsilon_0 = 1$   $\epsilon_f = 0.05$  respectively.

used in all DQNs agents started from  $\epsilon_0 = 1$  and decaying exponentially until  $\epsilon = 0.01$ . Figure 5 illustrates the epsilon  $\epsilon$  greedy values utilized in the DQN agents. The initial and final greedy values were  $\epsilon_0 = 1$  and  $\epsilon_f = 0.05$ , respectively, allowing 80 episodes of exploration and 420 episodes for exploitation. Figure 7 depicts one instance of the simulated random wave and the correspondent energy spectrum using

TABLE I: Agent Parameters.

Hyper parameters	DQN	Double DQN	Dueling DQN	PPO
Learning Rate (Both)	0.00001	0.00001	0.00001	0.0003
Batch size (Both)	64	64	64	5
Discount (Both)	0.995	0.995	0.995	0.99
Memory (Both)	10000	10000	10000	10000
Target Syn Frequency (DQNs)	10	10	10	-
Soft Update Weight (DQNs)	0.8	0.8	0.8	-
Gradient Clipping Value (DQNs)	1	1	1	-
Learning warm start (DQNs)	200	200	200	-
Likelihood Ratio Clipping (PPO)	-	-	-	0.2
Learning Frequency (PPO)	-	-	-	20
Learning Epochs (PPO)	-	-	-	4
GAE Lambda value (PPO)	-	-	-	0.95

TABLE II: Neural Network Parameters.

Network shape	DQN	Double DQN	Dueling DQN	PPO
Input Layer Neurons	1	1	1	1
Input Layer Activation Function	Tanh	Tanh	Tanh	Tanh
First Hidden Layer Activation Neurons	32	32	32	32
Second Hidden Layer Activation Function	Tanh	Tanh	Tanh	Tanh
Second Hidden Layer Neurons	32	32	32	32
Third Hidden Layer Activation Function	Tanh	Tanh	Tanh	Tanh
Third Hidden Layer Neurons	16	16	16	16
Output Layer Neurons	3	3	3	1
Output Layer Activation Function	-	-	-	Softmax

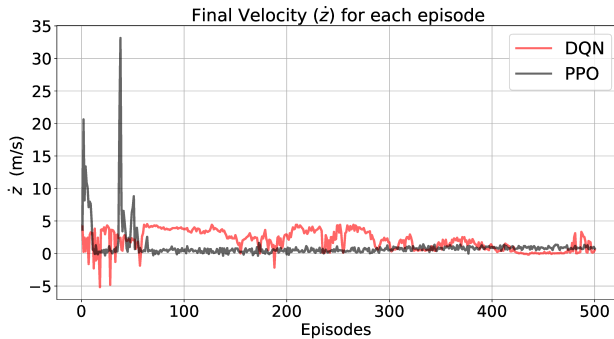


Fig. 6: A comparison between the final Impact Velocity  $\dot{z}$  of the VTOL-UAV in the case of PPO and DQN agents.

the JONSAWP model. At each episode, a new randomized simulated wave is generated to enhance the generalization of the policy for sim-to-real transfer. The learning rates  $\alpha$  used to update the policy of the DQN agents was  $\alpha = 0.0001$  based on the gradient of the loss function in Eq. (17) and (19). The learning rates  $\alpha_{\text{actor}}$  and  $\alpha_{\text{critic}}$  used to update the policy based on the loss function in Eq. (23) was  $\alpha_{\text{actor}} = \alpha_{\text{critic}} = 0.0003$ . A gradient clipping value of 1 is used in the case of the DQN, to guarantee a stable performance of the DQN agents.

A likelihood ratio clipping of 0.2 was used for the PPO agent with a learning Frequency of 20. The shape of the neural networks in all the agents is kept the same for the sake of fair comparison between the agents. The neural networks contained three layers with 32, 32, and 16 neurons. The hyperbolic tan function was utilized as the activation layer for all the layers. The remaining hyperparameters and neural network structure are shown in Table I and Table II.

Figure 6 illustrates the difference between the final impact velocity in the case of PPO (shown in black) and the DQN agent (shown in red). The PPO agent was able to learn better policy to track the required velocity  $\dot{z}_d$ . An exponential decay function was utilized to represent the required velocity  $\dot{z}_{2d}$ . Figure 8(a) compares the number of time steps needed to land between DQN and PPO agents. The number of steps needed by the PPO agent to land is lower than the DQN agents. The PPO agent was able to learn more efficient policies that require less steps to land compared to the DQN agents. Figure 8(b) illustrates the actor and critic loss moving average value of the PPO agent. The PPO agent showed smooth learning capabilities, where both actor and critic values converge to zero in less than 200 episodes. Figure 8(c) depicts the moving average value of the DQN agents for 500 episodes. Unlike the PPO, the moving average loss value of the DQN agents suffered from strong

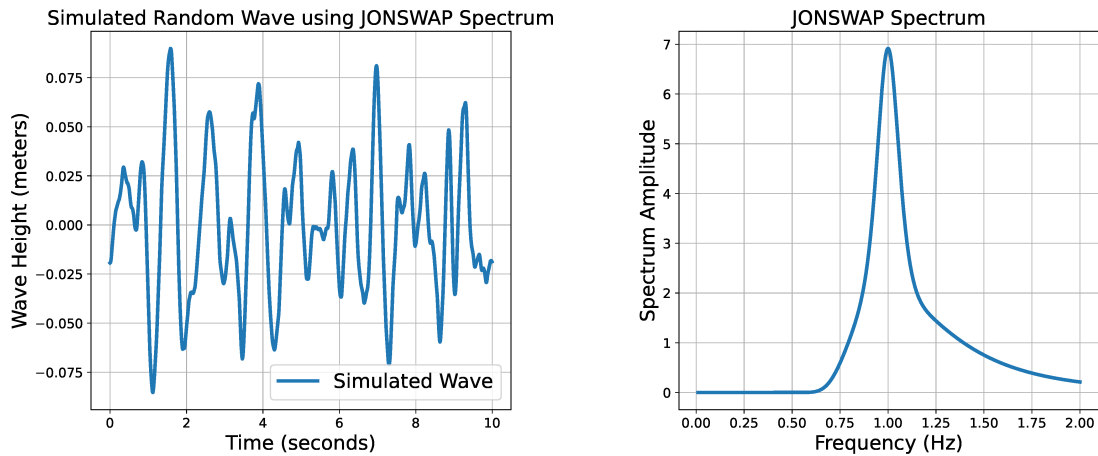


Fig. 7: The left portion of the figure depicts one instance of the simulated random wave using the JONSWAP model. At each episode, a new randomized simulated wave is generated to enhance the generalization of the policy for sim-to-real transfer. The right portion shows the energy spectrum of the same simulated wave.

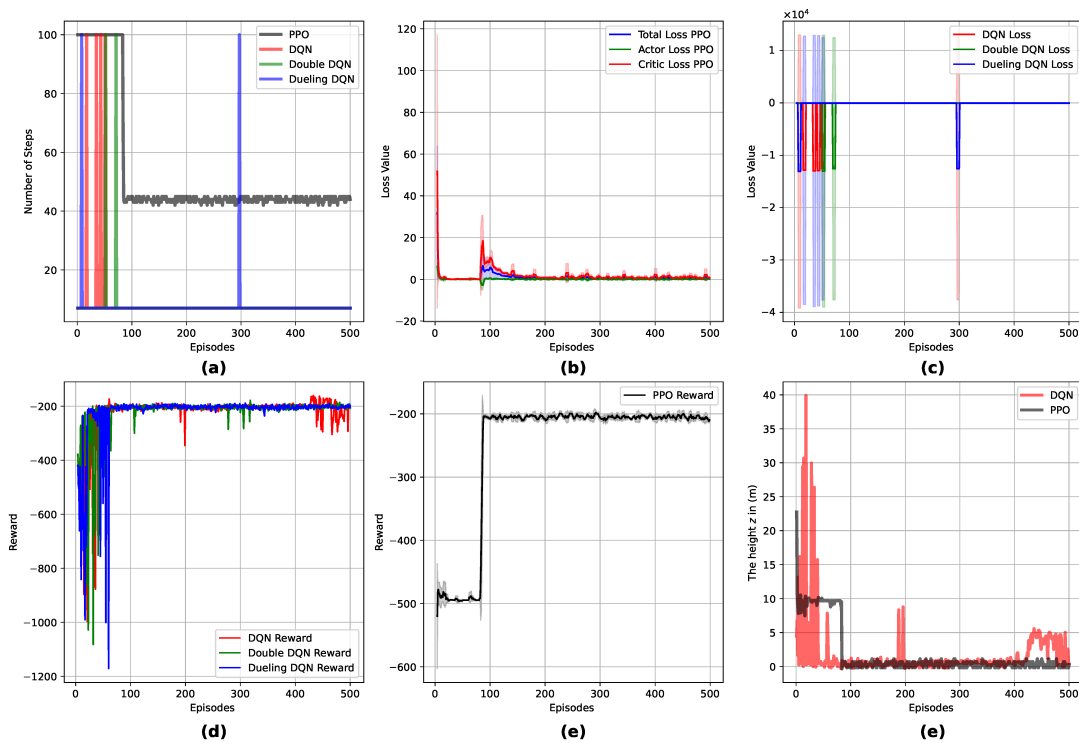


Fig. 8: Part (a) compares the number of time steps needed to land for all the agents. Part (b) illustrates the actor and critic loss moving average value of the PPO agent, while part (c) shows the moving average loss value of the DQNs agents. Part (d) and (e) depict the moving average of the reward of DQNs and PPO agents respectively. Finally, part (f) compares the final height achieved by DQN and PPO agents. The shaded parts in all figures represent the standard deviation of the moving average.

fluctuations, especially during the exploration phase. Figure 8(d) illustrates the moving average reward of the DQN agents. The DQN agent suffered from the forgetting phenomenon, where the agent forgot the optimal policy at the end of the

training. This phenomenon is usually related to overfitting. The Double DQN showed better performance compared to the normal and Dueling DQN. Figure 8(d) depicts the moving average reward value of the PPO agent. The PPO agent average

reward converged to a value around  $-200$  similar to the DQN agents. We experienced less sensitivity of the hyperparameters in the case of the PPO agent compared to the DQN. The performances of the agents have been evaluated in Table III in terms of final impact velocity, the time needed to land, and the inference time (computational time to recall the solution). The PPO agent was able to achieve the least value of final impact velocity due to its complicated and efficient policy compared to the DQNs. Due to its complicated policy, the PPO agent has the longest time to land compared to the DQN agents with 4.9 seconds.

TABLE III: Evaluation of the trained agents.

	Impact Velocity (m/s)	Time to Land (s)	Inference Time (ms)
PPO	0.327	<b>4.9</b>	<b>6.788</b>
DQN	0.820	5.4	9.854
Double DQN	<b>0.223</b>	7.7	7.220
Dueling DQN	2.419	6.3	11.296

## V. CONCLUSIONS & FUTURE WORK

A novel reinforcement learning approaches for sim-to-real policy transfer for Vertical Take-Off and Landing Unmanned Aerial Vehicle (VTOL-UAV) designed for landing on offshore docking stations in maritime operations has been proposed. The Joint North Sea Wave Project (JONSWAP) spectrum model has been employed to create a wave model for each episode, enhancing policy generalization for sim-to-real transfer. A set of DRL algorithms has been tested through numerical simulations including value-based agents such as Deep  $Q$  Networks (DQN) and policy-based agents such as Proximal Policy Optimization (PPO). The PPO agent achieved more stable and efficient learning to land in uncertain environments, which in turn enhances the likelihood of successful Sim-to-Real transfer. The simulation showed the capability of PPO to learn more complicated policies which turned out to be more efficient than the DQN policies. The learned policy can be utilized in real-time for control in the landing phase, where the policy will map the current state to optimal control action which has been learned through offline experience. For future work, exploring how agents perform with visual feedback from the on-board camera could be an intriguing area of investigation.

## ACKNOWLEDGMENTS

This work was supported in part by the National Sciences and Engineering Research Council of Canada (NSERC), under the grants RGPIN-2022-04937.

## REFERENCES

[1] H. A. Hashim, "Special orthogonal group SO (3), euler angles, angle-axis, rodriguez vector and unit-quaternion: Overview, mapping and challenges," *arXiv preprint arXiv:1909.06669*, 2019.

[2] P. Zieliński and U. Markowska-Kaczmar, "3d robotic navigation using a vision-based deep reinforcement learning model," *Applied Soft Computing*, vol. 110, p. 107602, 2021.

[3] L. Gupta, R. Jain, and G. Vaszkun, "Survey of important issues in uav communication networks," *IEEE Communications Surveys*, vol. 18, no. 2, pp. 1123–1152, 2016.

[4] L. Traub, "Validation of endurance estimates for battery powered uavs," *The Aeronautical Journal*, vol. 117, no. 1197, pp. 1155–1166, 2013.

[5] H. Shakhatareh, A. H. Sawalmeh, A. Al-Fuqaha, Z. Dou, E. Almaita, I. Khalil, N. S. Othman, A. Khreishah, and M. Guizani, "Unmanned aerial vehicles (uavs): A survey on civil applications and key research challenges," *IEEE Access*, vol. 7, pp. 48 572–48 634, 2019.

[6] J. Papayanopoulos, K. Webb, and J. Rogers, "An autonomous docking mechanism for vertical lift unmanned aircraft," *Journal of Mechanisms and Robotics*, vol. 11, no. 6, p. 061009, 2019.

[7] P. Cao, Y. Lu, H. Zhang, J. Li, W. Chai, C. Cai, and S. Wu, "Embedded lightweight squirrel-cage receiver coil for drone misalignment-tolerant wireless charging," *IEEE Transactions on Power Electronics*, vol. 38, no. 3, pp. 2884–2888, 2023.

[8] S. Wu, C. Cai, X. Liu, W. Chai, and S. Yang, "Compact and free-positioning omnidirectional wireless power transfer system for unmanned aerial vehicle charging applications," *IEEE Transactions on Power Electronics*, vol. 37, no. 8, pp. 8790–8794, 2022.

[9] J. M. Arteaga, S. Aldhafer, G. Kkelis, C. Kwan, D. C. Yates, and P. D. Mitcheson, "Dynamic capabilities of multi-mhz inductive power transfer systems demonstrated with batteryless drones," *IEEE Transactions on Power Electronics*, vol. 34, no. 6, pp. 5093–5104, 2019.

[10] S. Obayashi, Y. Kanekiyo, K. Nishizawa, and H. Kusada, "85-khz band 450-w inductive power transfer for unmanned aerial vehicle wireless charging port," in *2019 IEEE Wireless Power Transfer Conference (WPTC)*, 2019, pp. 80–84.

[11] H. Liu and X. Chen, "An unmanned aerial vehicle wireless charging system using a novel coupling structure," in *2022 IEEE 5th International Electrical and Energy Conference (CIEEC)*, 2022, pp. 2494–2499.

[12] Y. Shao, R. Ma, H. Zhang, M. Liu, and C. Ma, "Circuit architecture and design of a megahertz wireless power transfer system for drones," in *2022 International Power Electronics Conference (IPEC-Himeji 2022-ECCE Asia)*, 2022, pp. 63–67.

[13] T. Campi, S. Cruciani, G. Rodríguez, and M. Feliziani, "Coil design of a wireless power transfer charging system for a drone," in *2016 IEEE Conference on Electromagnetic Field Computation (CEFC)*, 2016, pp. 1–1.

[14] Z. Bie, J. Zhang, K. Song, D. Wang, and C. Zhu, "A free-rotation asymmetric magnetic coupling structure of uav wireless charging platform with conformal pickup," *IEEE Transactions on Industrial Electronics*, vol. 69, no. 10, pp. 10 154–10 161, 2022.

[15] L. Lan, C. H. Kwan, J. M. Arteaga, D. C. Yates, and P. D. Mitcheson, "A 100w 6.78mhz inductive power transfer system for drones," in *2020 14th European Conference on Antennas and Propagation (EuCAP)*, 2020, pp. 1–4.

[16] P. Cao, Y. Lu, H. Zhang, J. Li, W. Chai, C. Cai, and S. Wu, "Embedded lightweight squirrel-cage receiver coil for drone misalignment-tolerant wireless charging," *IEEE Transactions on Power Electronics*, vol. 38, no. 3, pp. 2884–2888, 2023.

[17] H. A. Hashim, A. E. Eltoukhy, and K. G. Vamvoudakis, "UWB ranging and IMU data fusion: Overview and nonlinear stochastic filter for inertial navigation," *IEEE Transactions on Intelligent Transportation Systems*, 2023.

[18] A. M. Ali, H. A. Hashim, and C. Shen, "Mpc based linear equivalence with control barrier functions for VTOL-UAVs," in *2024 IEEE American Control Conference (ACC)*, 2024, pp. 1–6.

[19] B. Herissé, T. Hamel, R. Mahony, and F.-X. Russotto, "Landing a vtol unmanned aerial vehicle on a moving platform using optical flow," *IEEE Transactions on Robotics*, vol. 28, no. 1, pp. 77–89, 2012.

[20] A. Paris, B. T. Lopez, and J. P. How, "Dynamic landing of an autonomous quadrotor on a moving platform in turbulent wind conditions," in *2020 IEEE International Conference on Robotics and Automation (ICRA)*, 2020, pp. 9577–9583.

[21] D. Falanga, A. Zanchettin, A. Simovic, J. Delmerico, and D. Scaramuzza, "Vision-based autonomous quadrotor landing on a moving platform," in *2017 IEEE International Symposium on Safety, Security and Rescue Robotics (SSRR)*, 2017, pp. 200–207.

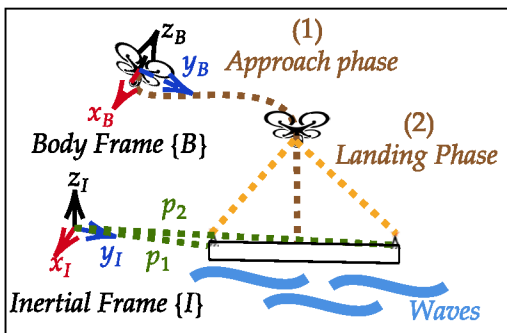
[22] "Autonomous landing of a multirotor micro air vehicle on a high velocity ground vehicle\* this work was partially supported by cfi jelf award 32848 and a hardware donation from dji." *IFAC-PapersOnLine*, vol. 50, no. 1, pp. 10 488–10 494, 2017, 20th IFAC World Congress.

- [23] J. S. Wynn and T. W. McLain, "Visual servoing with feed-forward for precision shipboard landing of an autonomous multicopter," in *2019 American Control Conference (ACC)*, 2019, pp. 3928–3935.
- [24] C. Yan, G. Chen, Y. Li, F. Sun, and Y. Wu, "Immune deep reinforcement learning-based path planning for mobile robot in unknown environment," *Applied Soft Computing*, vol. 145, p. 110601, 2023.
- [25] K. Arulkumaran, M. P. Deisenroth, M. Brundage, and A. A. Bharath, "Deep reinforcement learning: A brief survey," *IEEE Signal Processing Magazine*, vol. 34, no. 6, pp. 26–38, 2017.
- [26] T. T. Nguyen, N. D. Nguyen, and S. Nahavandi, "Deep reinforcement learning for multiagent systems: A review of challenges, solutions, and applications," *IEEE transactions on cybernetics*, vol. 50, no. 9, pp. 3826–3839, 2020.
- [27] M. I. Abouheaf, H. A. Hashim, M. A. Mayyas, and K. G. Vamvoudakis, "An online model-following projection mechanism using reinforcement learning," *IEEE Transactions on Automatic Control*, 2023.
- [28] V. Kumar, S. Shivram, S. Shah, D. Mahajan *et al.*, "Deep reinforcement learning with reward shaping for tracking control and vibration suppression of flexible link manipulator," *Applied Soft Computing*, p. 110756, 2023.
- [29] J. Garcia and F. Fernández, "A comprehensive survey on safe reinforcement learning," *Journal of Machine Learning Research*, vol. 16, no. 1, pp. 1437–1480, 2015.
- [30] S. Levine, N. Wagener, and P. Abbeel, "Learning contact-rich manipulation skills with guided policy search," 2015.
- [31] S. Levine, P. Pastor, A. Krizhevsky, J. Ibarz, and D. Quillen, "Learning hand-eye coordination for robotic grasping with deep learning and large-scale data collection," *The International journal of robotics research*, vol. 37, no. 4-5, pp. 421–436, 2018.
- [32] S. Levine, C. Finn, T. Darrell, and P. Abbeel, "End-to-end training of deep visuomotor policies," *The Journal of Machine Learning Research*, vol. 17, no. 1, pp. 1334–1373, 2016.
- [33] X. B. Peng, M. Andrychowicz, W. Zaremba, and P. Abbeel, "Sim-to-real transfer of robotic control with dynamics randomization," in *2018 IEEE international conference on robotics and automation (ICRA)*. IEEE, 2018, pp. 3803–3810.
- [34] J. Tobin, R. Fong, A. Ray, J. Schneider, W. Zaremba, and P. Abbeel, "Domain randomization for transferring deep neural networks from simulation to the real world," in *2017 IEEE/RSJ international conference on intelligent robots and systems (IROS)*. IEEE, 2017, pp. 23–30.
- [35] J. Tan, T. Zhang, E. Coumans, A. Iscen, Y. Bai, D. Hafner, S. Bohez, and V. Vanhoucke, "Sim-to-real: Learning agile locomotion for quadruped robots," *arXiv preprint arXiv:1804.10332*, 2018.
- [36] R. Julian, E. Heiden, Z. He, H. Zhang, S. Schaal, J. Lim, G. Sukhatme, and K. Hausman, "Scaling simulation-to-real transfer by learning composable robot skills," in *Proceedings of the 2018 International Symposium on Experimental Robotics*. Springer, 2020, pp. 267–279.
- [37] F. Golemo, A. A. Taiga, A. Courville, and P.-Y. Oudeyer, "Sim-to-real transfer with neural-augmented robot simulation," in *Conference on Robot Learning*. PMLR, 2018, pp. 817–828.
- [38] P. Christiano, Z. Shah, I. Mordatch, J. Schneider, T. Blackwell, J. Tobin, P. Abbeel, and W. Zaremba, "Transfer from simulation to real world through learning deep inverse dynamics model," *arXiv preprint arXiv:1610.03518*, 2016.
- [39] A. A. Rusu, M. Večerík, T. Rothörl, N. Heess, R. Pascanu, and R. Hadsell, "Sim-to-real robot learning from pixels with progressive nets," in *Conference on robot learning*. PMLR, 2017, pp. 262–270.
- [40] J. Hwangbo, I. Sa, R. Siegwart, and M. Hutter, "Control of a quadrotor with reinforcement learning," *IEEE Robotics and Automation Letters*, vol. 2, no. 4, pp. 2096–2103, 2017.
- [41] W. Koch, R. Mancuso, R. West, and A. Bestavros, "Reinforcement learning for uav attitude control," *ACM Transactions on Cyber-Physical Systems*, vol. 3, no. 2, pp. 1–21, 2019.
- [42] Y. Bicer, M. Moghadam, C. Sahin, B. Eroglu, and N. K. Üre, "Vision-based uav guidance for autonomous landing with deep neural networks," in *AIAA Scitech 2019 Forum*, 2019, p. 0140.
- [43] R. Polvara, M. Patacchiola, S. Sharma, J. Wan, A. Manning, R. Sutton, and A. Cangelosi, "Toward end-to-end control for uav autonomous landing via deep reinforcement learning," in *2018 International conference on unmanned aircraft systems (ICUAS)*. IEEE, 2018, pp. 115–123.
- [44] R. Polvara, S. Sharma, J. Wan, A. Manning, and R. Sutton, "Autonomous vehicular landings on the deck of an unmanned surface vehicle using deep reinforcement learning," *Robotica*, vol. 37, no. 11, pp. 1867–1882, 2019.
- [45] J. E. Kooi and R. Babuška, "Inclined quadrotor landing using deep reinforcement learning," in *2021 IEEE/RSJ International Conference on Intelligent Robots and Systems (IROS)*. IEEE, 2021, pp. 2361–2368.
- [46] R. S. Sutton and A. G. Barto, *Reinforcement Learning: An Introduction*. A Bradford Book, 2018.
- [47] V. Mnih, K. Kavukcuoglu, D. Silver, A. Graves, I. Antonoglou, D. Wierstra, and M. Riedmiller, "Playing atari with deep reinforcement learning," *arXiv preprint arXiv:1312.5602*, 2013.
- [48] H. A. Hashim, A. E. Eltoukhy, and A. Odry, "Observer-based controller for VTOL-UAVs tracking using direct vision-aided inertial navigation measurements," *ISA transactions*, vol. 137, pp. 133–143, 2023.
- [49] H. A. Hashim, "Exponentially stable observer-based controller for VTOL-UAVs without velocity measurements," *International Journal of Control*, vol. 96, no. 8, pp. 1946–1960, 2023.
- [50] T. E. Oliphant, "Python for scientific computing," *Computing in science & engineering*, vol. 9, no. 3, pp. 10–20, 2007.
- [51] V. S. Kumar and K. A. Kumar, "Spectral characteristics of high shallow water waves," *Ocean Engineering*, vol. 35, no. 8-9, pp. 900–911, 2008.
- [52] R. S. Sutton and A. G. Barto, *Reinforcement learning: An introduction*. MIT press, 2018.
- [53] H. Van Hasselt, A. Guez, and D. Silver, "Deep reinforcement learning with double q-learning," in *Proceedings of the AAAI conference on artificial intelligence*, vol. 30, no. 1, 2016.
- [54] Z. Wang, T. Schaul, M. Hessel, H. Hasselt, M. Lanctot, and N. Freitas, "Dueling network architectures for deep reinforcement learning," in *International conference on machine learning*. PMLR, 2016, pp. 1995–2003.
- [55] J. Schulman, F. Wolski, P. Dhariwal, A. Radford, and O. Klimov, "Proximal policy optimization algorithms," *arXiv preprint arXiv:1707.06347*, 2017.
- [56] J. Schulman, P. Moritz, S. Levine, M. Jordan, and P. Abbeel, "High-dimensional continuous control using generalized advantage estimation," *arXiv preprint arXiv:1506.02438*, 2015.
- [57] J. Schulman, S. Levine, P. Abbeel, M. Jordan, and P. Moritz, "Trust region policy optimization," in *Proceedings of the 32nd International Conference on Machine Learning*, ser. Proceedings of Machine Learning Research, F. Bach and D. Blei, Eds., vol. 37. Lille, France: PMLR, 07–09 Jul 2015, pp. 1889–1897.

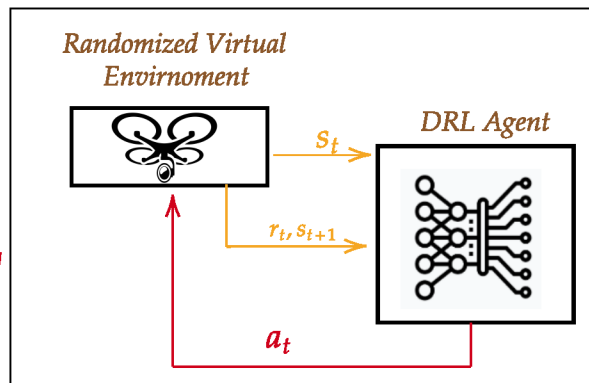
This figure "SGD.png" is available in "png" format from:

<http://arxiv.org/ps/2406.00887v1>

### VTOL-UAV Dynamic Modeling



### Training in Simulation



Sim-to-Real  
Transfer

### Real-time experiments

